Excited state absorption of Cr3 + in K2NaScF6 and Gd3Ga2(MO4)3, M=Ga, Al

Leonard J. Andrews, Stewart M. Hitelman, Milan Kokta, and David Gabbe

Citation: The Journal of Chemical Physics **84**, 5229 (1986); doi: 10.1063/1.449932
View online: http://dx.doi.org/10.1063/1.449932
View Table of Contents: http://scitation.aip.org/content/aip/journal/jcp/84/10?ver=pdfcov
Published by the AIP Publishing

Excited state absorption of Cr^{3+} in K_2NaScF_6 and $Gd_3Ga_2(MO_4)_3$, M = Ga, Al

Leonard J. Andrews and Stewart M. Hitelman[a)]
GTE Laboratories, Incorporated, Waltham, Massachusetts 02254

Milan Kokta
Union Carbide Corporation, Washougal, Washington 98671

David Gabbe
Crystal Physics and Optical Electronics Laboratory, Massachusetts Institute of Technology, Cambridge, Massachusetts 02139

(Received 16 January 1986; accepted 11 February 1986)

The excited state absorption (ESA) spectra of Cr^{3+} in the elpasolite K_2NaScF_6 and the garnets $Gd_3Sc_2(GaO_4)_3$ (GSGG) and $Gd_3Sc_2(AlO_4)_3$ (GSAG) were measured from 0.3 to 1.8 μ, exclusive of the fluorescence region, using pulsed laser excitation. The two ligand field transitions $^4T_{1g}(a) \leftarrow {}^4T_{2g}$ and $^4T_{1g}(b) \leftarrow {}^4T_{2g}$ were located in the garnets at 9000 and 19 400 cm^{-1} (19 200 cm^{-1} for the elpasolite). In addition, intense UV charge transfer bands were found in the garnets, but not the elpasolite. The elpasolite spectrum confirms that major differences exist between the ESA of ^2E_g and $^4T_{2g}$ Cr^{3+} excited states. A single configuration coordinate model is developed which is adequate for predicting energies but not the bandwidths of ^2E_g and $^4T_{2g}$ ESA transitions between ligand field levels.

I. INTRODUCTION

An underdeveloped area in the optical spectroscopy of fluorescent transition metal ions is excited state absorption (ESA). A knowledge of ESA is of interest not only because it provides fundamental information regarding the nature of higher lying excited states often inaccessible from the ground state, but also because it can provide information critical to assessing the lasing potential of fluorescent ions. Indeed, the current lack of realistic models and paucity of data are major impediments to the development of tunable solid state lasers, a task which requires detailed knowledge of ESA processes in order to understand and predict lasing properties. For these reasons, a study was undertaken of the ESA of low field Cr^{3+}, an ion which has played a key role in advancing the understanding of the transition metal optical spectroscopy.

It is well established that trivalent chromium in octahedral coordination can have either a ^2E_g or a $^4T_{2g}$ lowest excited state and that the identity of the lowest excited state is dependent on the strength of the ligand field at the Cr^{3+} site.[1] There have been several reports of the ESA of high field Cr^{3+} which characterized electronic transitions of the type higher states$\leftarrow {}^2E_g$ [2-6] including the definitive work by Fairbank *et al.*[2] on ruby, emerald, and MgO:Cr^{3+}, and the more recent studies on tunable laser material alexandrite by Shand *et al.*[3,4] On the other hand, no thorough study has appeared on the ESA of low field Cr^{3+} which has transitions of the type higher states$\leftarrow {}^4T_{2g}$. Consideration of the spin selection rule for electronic transitions leads to the conclusion that major differences should exist between the ESA spectra of ^2E_g and $^4T_{2g}$ excited states of a d^3 ion. One of our present purposes is to verify this conclusion by measuring the ESA of Cr^{3+} in low field hosts over a wide spectral range and make a comparison with the prior work on Cr^{3+} in high field hosts. For this study, the oxide garnets GSGG [$Gd_3Sc_2(GaO_4)_3$] and GSAG [$Gd_3Sc_2(AlO_4)_3$] and the fluoride elpasolite K_2NaScF_6 were chosen as the low field Cr^{3+} hosts. The garnets are of technological interest because tunable lasing on the $^4T_{2g} \rightarrow {}^4A_{2g}$ transition has been demonstrated in them[7]; however the elpasolite is of particular theoretical interest because its spectrum can be interpreted in a straightforward manner uncomplicated by the intense charge transfer transitions that we have found present in the oxides. Our second purpose is to compare high and low field Cr^{3+} ESA spectra with a simple single configuration coordinate ligand field model to assess the usefulness of this semiclassical approach for predicting the salient features of ESA transitions between ligand field states of transition metal ions.

The remainder of this paper is organized as follows: experimental details are given in Sec. II, the available spectroscopic evidence establishing the Cr^{3+} excited state level ordering is summarized in Sec. III, excited state difference spectra and cross sections derived from them are in Secs. IV and Sec. V, the long wavelength tuning limit of the GSGG:Cr laser is deduced in Sec. VI, the single configuration coordinate model for Cr^{3+} ESA is developed in Sec. VII, and finally, Sec. VIII briefly discusses the findings of this study.

II. MATERIALS AND APPARATUS

$Gd_3Sc_2(GaO_4)_3$ (GSGG) and $Gd_3Sc_2(AlO_4)_3$ (GSAG) are cubic garnets belonging to space group O_h^{10}. The dopant Cr^{3+} is substantially incorporated into the octahedral Sc^{3+} sites which have a strong trigonal distortion and site symmetry S_6 ($= C_3 \times i$). Both garnets were grown by the Czochralski method at Union Carbide with 1.0 at. % Cr^{3+} doping. The cell constant for GSGG is 1.255 nm[8] which gives an Sc^{3+} ion density of $16/a_0^3 = 8.1 \times 10^{21}$ cm^{-3}. The density of a cut and polished GSGG sample was measured to be 2.48 g cm^{-3} which corre-

[a)] Present address: Department of Applied Physics, Cornell University, Ithaca, New York.

 0021-9606/86/105229-10$02.10

sponds to an Sc^{3+} ion density of 8.0×10^{21} cm^{-3}. Using 8.1×10^{-19} cm^{-3} as the Cr^{3+} density, the absorption cross section at the ${}^4T_{2g}\leftarrow{}^4A_{2g}$ peak was calculated to be 2.7×10^{-20} cm^2 for GSGG:Cr^{3+} at 290 K.

K_2NaScF_6 crystallizes with the cubic elpasolite (also known as ordered perovskite) structure and belongs to space group O_h^5. Cr^{3+} ion occupies the Sc^{3+} sites which have full O_h site symmetry. The elpasolite:Cr^{3+} was grown at MIT in a closed vessel by Czochralski with a Cr^{3+} doping of 2.5 at. %. The unit cell constant is 0.846 nm, and the corresponding Sc^{3+} ion density is $4/a_0^3 = 6.6\times10^{21}$ cm^3. This yields a Cr^{3+} density of 1.7×10^{20} cm^{-3} and a peak ${}^4T_{2g}\leftarrow{}^4A_{2g}$ cross section of 1.2×10^{-20} cm^2 at 290 K.

Fluorescence spectra were excited at 568.2 nm with a Kr ion laser, and measured with a SPEX 1402 double monochromator and a cooled (− 100 °C) RCA 7102 phototube both interfaced to a DG Eclipse S/120 computer. The spectral response of the fluorimeter was calibrated with a standard 1 kW tungsten–halogen lamp. Fluorescence lifetimes were measured at the peak of the emission band using photon counting with a Nicolet 1170 multichannel analyzer also interfaced to the S/120, and a PRA 1762/1763 amplifier discriminator. Sample cooling was provided by a cold N_2 flow or a Janis liquid He crysostat and heating by a small resistance muffle furnace with optical access. Fluorescence decays were always exponential and were usually monitored over three decades except at elevated temperatures where interference from the thermal background degraded the S/N ratio. The refractive index of GSGG:Cr^{3+} at 632.8 nm (1.94) was calculated from the orientation required to achieve Brewster's angle ($n = \tan\theta_B$) for a polished GSGG:Cr^{3+} slab in a laser cavity. Absorption spectra were measured on a Cary 17D spectrometer.

The ESA measurements were performed with a transversely oriented pump–probe apparatus consisting of Candela coaxial flashlamp dye laser pump (Kiton Red 620, 628 nm, 0.85 μs), a pulse intensified Xe arc probe (150 W, 20×, 2 ms), a Spex 1680B double monochromator, and either an RCA4832 GaAs phototube or a Judson J16-TE200 Ge diode detector. The output of the detector was amplified and recorded with the Nicolet 1170. The garnets were high optical quality crystals cut and polished for 1 cm probe paths. The elpasolite was a small, lower optical quality crystal cut for 0.5 cm probe path. ESA spectral measurements were performed with the unfocused dye laser (1.0 cm beam diameter) operated at 1 J, or about 1.5 MW/cm^2. If it is assumed that the specific heat for YAG (0.15 cal g^{-1} K^{-1}) is appropriate for the materials used here, the temperature rise per pulse is only 0.6 K. In the $\Delta\alpha$ vs power experiments described later, the pump was focused with a cylindrical lens and the pump pulse spatial profile was mapped by translating the HeNe probe beam both vertically and horizontally through the sample. It was found that careful dye laser alignment and a low dye concentration (0.1 g/ℓ) were necessary to obtain a well-behaved pump beam profile free of hot spot discontinuities. Typical operating parameters were 0.1 cm beam width and 0.3 J pump energy which corresponds to less than 5 MW/cm^2 pulse intensity and a 1.5 K temperature rise.

III. IDENTITY OF THE Cr^{3+} LOWEST EXCITED STATE

Since one of the goals of this work is to measure the ESA spectrum of the ${}^4T_{2g}$ state of Cr^{3+}, it is important to establish the Cr^{3+} excited state level ordering in our hosts. In the case of the elpasolite:Cr^{3+}, the 290 K emission consists of a broad featureless band typical of ${}^4T_{2g}\rightarrow{}^4A_{2g}$ fluorescence with no trace of the sharp structure characteristic of ${}^2E_g\rightarrow{}^4T_{2g}$ phosphorescence.[1] This implies that the ${}^4T_{2g}$ may be the lowest excited state and is consistent with the other available evidence which places the ${}^2E_g$ energetically well above the ${}^4T_{2g}$. Specifically, the ${}^4T_{2g}\leftarrow{}^4A_{2g}$ zero phonon line at 4 K appears prominently in emission and weakly in absorption at 14 530 cm^{-1}.[9] At higher temperatures, it is likely that the zero phonon line will red shift due to lattice expansion. On the other hand, the ${}^2E_g\leftarrow{}^4A_{2g}$ zero phonon line cannot be reliably positioned because only a broad antiresonance notch is observable in absorption in the vicinity of the expected ${}^2E_g$ position at all temperatures, and ${}^2E_g$ emission has never been observed at ambient pressure. Fortunately, high pressure 290 K luminescence measurements have recently been performed on the elpasolite, and the ${}^2E_g\rightarrow{}^4A_{2g}$ zero phonon line was clearly observed in emission at 15 150 cm^{-1}.[10] Furthermore, the position of the ${}^2E_g$ zero phonon line was found to be quite insensitive to pressure changes indicating that the Racah interelectronic repulsion parameters (B and C) are only weakly perturbed by small changes in the lattice constant.[10] From these data, we conclude that at 290 K the ${}^2E_g$ lies at least 600 cm^{-1} above the ${}^4T_{2g}$ in the elpasolite, and that, after taking degeneracies into account, this corresponds to a minimum of 98% ${}^4T_{2g}$ excited state population when the excited ion is thermally equilibrated.

The emission of Cr^{3+} in GSGG also consists of a featureless broad band virtually indistinguishable from its emission in the elpasolite. If the first and second moments, m_1 and m_2, of the normalized fluorescence $f(\bar\nu)$ are defined as in Eqs. (2) and (3), then the first moments are the same in each host, 12 900 cm^{-1}, and the second moments differ by only 2%, 7.65×10^5 (GSGG) and 7.81×10^5 cm^{-2} (elpasolite). This close correspondence

$$m_0 = \int_{-\infty}^{\infty} f(\bar\nu)\,d\bar\nu = 1, \tag{1}$$

$$m_1 = \langle\bar\nu\rangle = \int_0^{\infty} \bar\nu f(\bar\nu)\,d\bar\nu, \tag{2}$$

$$m_2 = \langle\bar\nu - \langle\bar\nu\rangle\rangle^2 = \int_{-\infty}^{\infty} (\bar\nu - \langle\bar\nu\rangle)^2 f(\bar\nu)\,d\bar\nu \tag{3}$$

is a consequence of the similar 10 Dq values for Cr^{3+} in these hosts, 15 550 (GSGG) and 15 600 cm^{-1} (elpasolite), but it must also reflect nearly identical ${}^4T_{2g}$ coupling to each lattice. In spite of these similarities, the ${}^2E_g - {}^4T_{2g}$ separations are not expected to be the same because Racah parameters differ between oxides and fluorides. In fact, the recently reported[11] 4 K luminescence of GSGG:Cr^{3+} shows dual emission from both the ${}^2E_g$ and ${}^4T_{2g}$ states with the broadband quartet fluorescence dominant. This can only result from two levels which are at most a few tens of wave numbers apart, although without more data the level ordering and

precise level separation cannot be established. At 290 K, the populations of these states can therefore be expected to be determined by the ratio of degenericies, i.e., 3/1. This high $^4T_{2g}$ population is consistent with the complete absence of fine structure in the 290 K luminescence which implies little emission intensity from the ^2E_g state.

Little spectroscopic information is available for GSAG:Cr^{3+}, however the value for 10 Dq at 290 K is about 250 cm^{-1} greater than in GSGG:Cr^{3+} so that if the ^2E_g lies at approximately the same energy in both garnets, then GSAG can be expected to be a significantly high field host. Nevertheless, the 290 K luminescence is a broad featureless band which must be dominated by $^4T_{2g}$ fluorescence.

In order to better define the $^4T_{2g} - {}^2E_g$ level separation in the garnets, the temperature dependencies of their emission lifetimes were measured, and they are compared with elpasolite:Cr^{3+} in Fig. 1. The weakly temperature dependent increase in lifetime between 550 and 4 K for elpasolite:Cr^{3+} is attributable to a lengthening of the $^4T_{2g}$ radiative lifetime due to depopulation of intensity borrowing ungerade vibrations and possibly also to lattice contraction. Although the magnitudes of the radiative matrix elements differ somewhat between GSGG:Cr^{3+} and elpasolite:Cr^{3+}, the Cr^{3+} lifetime in the garnet exactly parallels the elpasolite data which confirms the interpretation that luminescence is dominated by $^4T_{2g}$ relaxation in GSGG even at 4 K where structure attributable to ^2E_g emission is seen.[11] The situation for GSAG:Cr^{3+} is analogous to the other hosts and only a small increase in lifetime occurs betwen 500 and 77 K reflecting the change in $^4T_{2g}$ radiative lifetime. This must mean that $^4T_{2g}$ cannot lie much more than kT at 77 K (53 cm^{-1}) above ^2E_g. However, a more definitive assessment of the level ordering must await lower temperature data which may reveal the influence of the ^2E_g state on the relaxation kinetics. For our present purpose of interpreting room temperature ESA data, the elpasolite spectrum can be regarded as reflecting an exclusively $^4T_{2g}$ initial state, whereas the garnet spectra are predominantly $^4T_{2g}$, i.e., 75%.

The sharp decrease in lifetimes which begins in the range 500–550 K in all hosts signals the onset of thermally activated radiationless relaxation and is treated in detail elsewhere.[12]

Finally, we note that the $^4T_{2g}$ fluorescence lifetimes at 290 K were measured to be 120, 160, and 280 μs for Cr^{3+} in GSGG, GSAG and K_2NaScF_6, respectively.

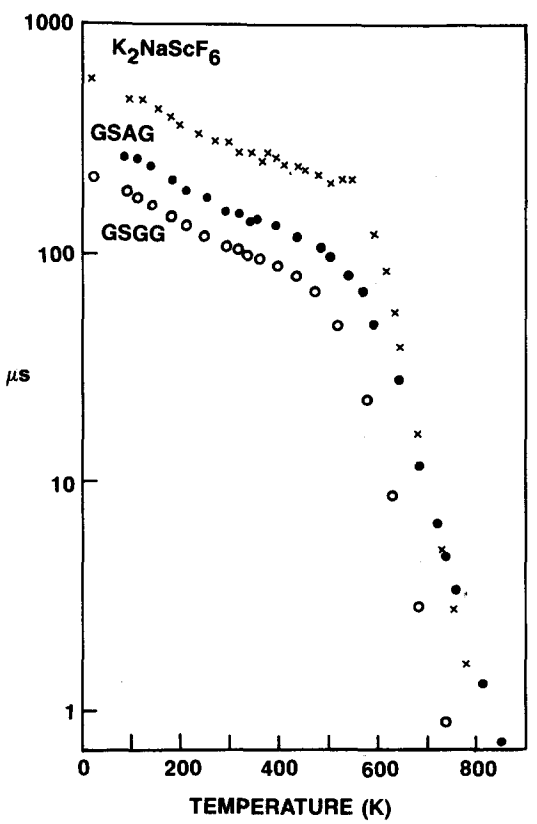

FIG. 1. Temperature dependence of the Cr^{3+} fluorescence lifetime in K_2NaScF_6, GSGG, and GSAG. The 4 K data point for GSGG is from Ref. 11.

IV. EXCITED STATE DIFFERENCE SPECTRA

The change in absorption $\Delta\alpha$ of a weak probe beam in an ESA experiment can be related to the transmitted probe intensities through the pumped and unpumped sample, I_p and I_u, and the probe path length in the sample l by Eq. (4),

$$\Delta\alpha = \ln_e(I_u/I_p)/l. \tag{4}$$

Should the absorption constant of the sample increase with optical pumping, then $\Delta\alpha$ as defined by Eq. (5) will be positive. The change in absorption $\Delta\alpha$ is also related to the ground and excited state cross sections, σ_0 and σ_1, and the excited state population n_1 by Eq. (5),

$$\Delta\alpha = (\sigma_1 - \sigma_0)n_1. \tag{5}$$

In Fig. 2 are shown the excited state difference spectrum ($\Delta\alpha$ vs wavelength) and the GSA spectrum of the same single crystal of Cr^{3+} doped elpasolite. A comparison of these spectra reveals that optical pumping causes bleaching ($\Delta\alpha < 0$) in the region of the $^4T_{2g}$, $^4T_{1g}(a) \leftarrow {}^4A_{2g}$ ground state transitions, whereas an ESA difference spectrum peak is located at 19 600 cm^{-1}. The position of this ESA band will

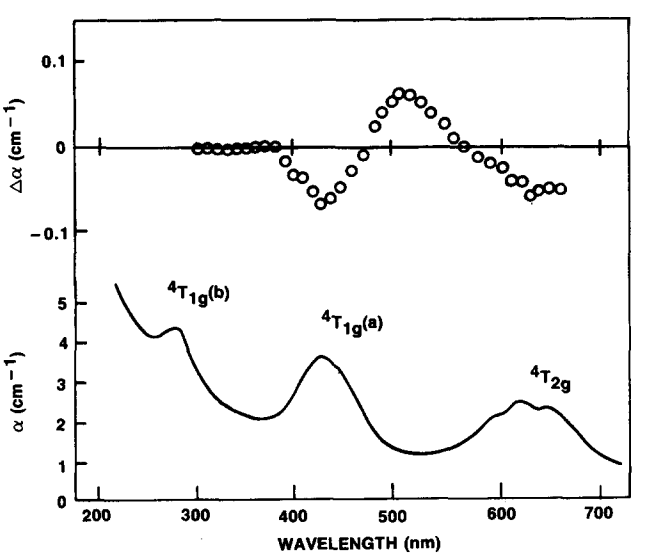

FIG. 2. The excited state difference spectrum (upper) and ground state absorption spectrum (lower) of Cr^{3+} in K_2NaScF_6.

be better characterized in Sec. VI where ESA cross sections are extracted from difference spectra; here we simply anticipate the later analysis by stating that the position and intensity of this ESA band identify it as the ${}^4T_{1g}(b) \leftarrow {}^4T_{2g}$ ligand field transition. Notice in Fig. 2 that no other ESA features are present up to 33 000 cm^{-1}, and furthermore, cruder measurements not shown in Fig. 2 reveal that no strong ESA is present up to at least 40 000 cm^{-1}. At its long wavelength edge, the ESA difference spectrum in Fig. 2 is truncated by instrumental limitations arising from the spontaneous emission of the sample which overwhelms the Xe arc probe beam in the fluorescence region. Sample fluorescence is not a problem below 10 000 cm^{-1}, so an attempt was made to measure ESA in the near infrared; however, low cross sections and a short sample path length resulted in $\Delta\alpha$ values below the apparatus detection limit of 0.01 cm^{-1}.

The ESA difference spectrum for Cr^{3+} in GSGG is similar to the elpasolite in the visible region, there is bleaching of the two lowest energy GSA quartet–quartet transitions and an ESA difference spectrum peak occurs at 18 700 cm^{-1}. However, there is a major difference in the UV ESA spectra for Cr^{3+} in oxide and fluoride hosts. While the UV is devoid of ESA for Cr^{3+} in the elpasolite, Fig. 3 shows that in both GSGG and GSAG an intense broad band dominates this spectral region. The peak cross section for this band is about 200 times larger than for the visible ligand field transitions, clearly indicating that it is electric dipole allowed. In addition, the search for a near infrared ESA transition was successful in GSGG:Cr^{3+} and a weak, complex band with a pronounced long wavelength shoulder was located with a peak near 9000 cm^{-1}. This is shown in the composite GSGG:Cr^{3+} ESA in Sec. VI, Fig. 8 where its position and intensity identifies it as the ${}^4T_{1g}(a) \leftarrow {}^4T_{2g}$ ligand field transition. In spite of the fact 25% of the excited state population of GSGG:Cr^{3+} is in the ${}^2E_g$ state, none of the fine structure

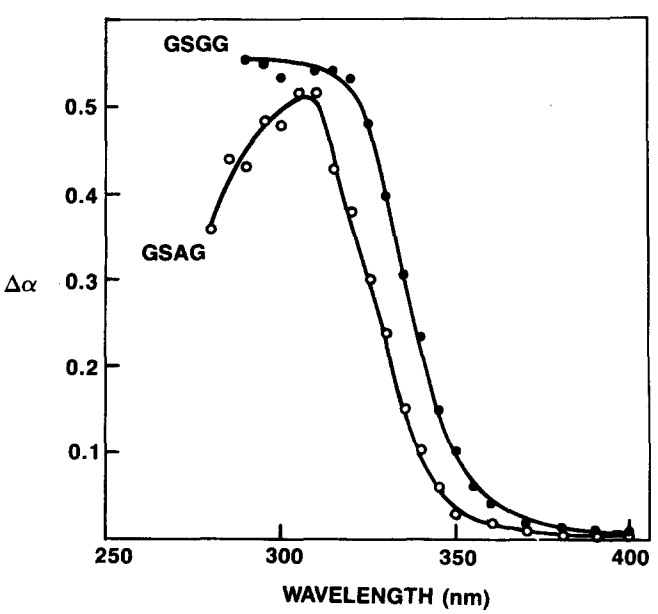

FIG. 3. The ultraviolet excited state difference spectrum of Cr^{3+} in GSAG and GSGG.

associated with the near infrared ESA of high field Cr^{3+} was evident in our data.[2] However, it is possible that the weak, long wavelength shoulder centered near 6500 cm^{-1} is attributable to the ${}^2T_{2g}(a) \leftarrow {}^2E_g(a)$ transition.

The ESA difference spectrum of GSAG:Cr^{3+} closely resembles GSGG:Cr^{3+} in the visible and near infrared, whereas Fig. 3 shows a blue shift of 800 cm^{-1} for the Cr^{3+} UV band in the aluminum garnet as compared with the gallium garnet. In these lattices, aluminum and gallium are next nearest neighbors of Cr^{3+}.

Finally, we note that all of the ESA features described here were found to decay exponentially with lifetimes which exactly matched the luminescent lifetimes of Cr^{3+} in each host.

V. EXCITED STATE ABSORPTION CROSS SECTIONS

According to Eq. (6), in order to extract the excited state cross sections from difference spectral data, it is necessary to know the ground state cross sections and the excited state population n_1. While σ_0 can be determined from the total active ion density and absorption constant, $\sigma_0 = \alpha/N$, obtaining the excited state population n_1 is less straightforward. We used two methods to measure n_1 for GSGG:Cr^{3+} which gave consistent results. First, the pump power dependence of the ${}^4T_{2g}$ bleaching was modeled by solving the appropriate rate equations. Initially, an attempt was made to saturate the bleaching (i.e., $n_1 = N$), but it was discovered that pump intensities in excess of 10 MW/cm^2 induced thermal lensing in GSGG:Cr^{3+} which forced us to restrict pump intensities in these experiments to 5 MW/cm^2 or less. As shown later, this is well below the intensity required for saturation, but it was found that n_1 could be extracted with reasonable precision by fitting data in the low power regime. Second, it was found that n_1 can be estimated to within $\pm$ 25% by simply plotting the quantity $\Delta\alpha/n_1 + \sigma_0 (= \sigma_1)$ vs wavelength and varying n_1 until physically meaningful results are obtained. If n_1 is chosen too large, then the calculated σ_1 spectrum has the appearance of the σ_0 spectrum. If n_1 is chosen too small, then σ_1 becomes negative over at least part of its range. This technique was originally described by Fairbank *et al.*[2] and used by these authors to deduce σ_1 in MgO:Cr^{3+}.

The three state model shown in Fig. 4 was used to calculate the variation of $\Delta\alpha$ with pump intensity for GSGG:Cr^{3+}. In Fig. 4, P is the pump intensity, τ_1 is the relaxation time of the luminescent level and τ_2 is the relaxation time of the ESA terminal level which corresponds to resonance with the pump laser. This system is described by the coupled equations (6) and (7),

$$dn_1/dt = \sigma_0 n_0 P - \sigma_1 n_1 P + n_2/\tau_2 - n_1/\tau_1, \tag{6}$$

$$dn_2/dt = \sigma_1 n_1 P - n_2/\tau_2. \tag{7}$$

The solutions for boundary conditions $N = n_0 + n_1 + n_2$ and $n_1 = n_2 = 0$ at $t = 0$ are given by Eqs. (8) and (9),

$$n_1 = \frac{\sigma_0 PN}{\lambda_+ - \lambda_-}\left[e^{\lambda_+ t} - e^{\lambda_- t}\right] + \frac{\sigma_0 PN}{\tau_2}\left[\frac{1}{\lambda_+\lambda_-} + \frac{1}{\lambda_+ - \lambda_-}\left(\frac{e^{\lambda_+ t}}{\lambda_+} - \frac{e^{\lambda_- t}}{\lambda_-}\right)\right], \tag{8}$$

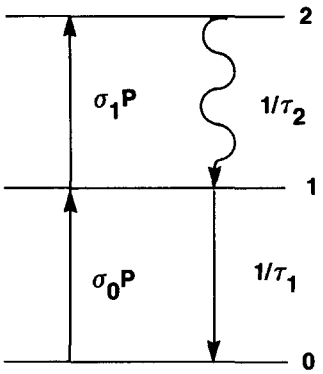

FIG. 4. Schematic diagram of the three level model used to calculate the pump power dependence of $\Delta\alpha$. The symbols for the rates are defined in the text.

$$n_2 = \sigma_0\sigma_1 P^2 N\left[\frac{1}{\lambda_+\lambda_-} + \frac{1}{\lambda_+ - \lambda_-}\left(\frac{e^{\lambda_+ t}}{\lambda_+} - \frac{e^{\lambda_- t}}{\lambda_-}\right)\right], \tag{9}$$

$$\begin{aligned} 2\lambda_\pm = &-[(\sigma_0+\sigma_1)P + 1/\tau_1 + 1/\tau_2] \\ &\pm \{[(\sigma_0+\sigma_1)P + 1/\tau_1 + 1/\tau_2]^2 \\ &+ 4(\sigma_1 P/\tau_2 - \sigma_1\sigma_0 P^2 \\ &- [(\sigma_0+\sigma_1)P + 1/\tau_1]/\tau_2)\}^{-1/2}. \end{aligned}$$

Of the parameters required to calculate n_1 using Eq. (8), only τ_2 and σ_1 are not known. If τ_2 is taken to be at least a factor of 10 faster than the 0.85 μs dye laser pump pulse duration, which it certainly must be, then the calculated value for n_1 was found to be sensibly independent of τ_2. This makes σ_1, the ESA cross section at the pump wavelength, the only fitted parameter required to model $\Delta\alpha$ vs P data at any probe wavelength. After specifying the pump σ_1, a set of n_1 values corresponding to the experimental P's is calculated. Using Eq. (6), this set of n_1's and the experimental $\Delta\alpha$'s were used to calculate σ_1 at the *probe* wavelength. Finally, σ_1 at pump wavelength was then varied to achieve the best self-consistent set of probe σ_1's. Figure 5 shows the data and fit for GSGG:Cr^{3+} using a 628 nm pump and a 632.8 nm HeNe laser probe. Using $\sigma_0 = 2.6\times10^{-20}$ cm^2 at 632.8 nm, the best value for σ_1 at 632.8 nm was found to be 0.55×10^{-20} cm^2 which corresponds to $n_1/N = 0.249$ at maximum pump intensity used in the measurement, 4.3 MW/cm^2. Armed with these values for σ_0 and σ_1 at the probe wavelength, it is now possible to determine n_1 from the $^4T_2$ bleaching in GSGG:Cr^{3+}. The dashed curve in Fig. 5 was calculated using Eq. (9) to show that saturation is expected to occur only at pump intensities in excess of 60 MW/cm^2, a factor of 15 greater than the maximum intensity used here.

The model shown in Fig. 4 assumes that level 2 relaxes only by repopulating level 1. While this is a likely occurrence in GSGG:Cr^{3+} pumped at 632.8 nm, the efficiency of the level 2→level 1 radiationless decay has not been measured, so the effect of relaxing this assumption on the modeling of $\Delta\alpha$ vs P data was investigated. This was done by simply making τ_2 long with respect to the pump pulse duration, and calculating n_1 at the end of the pump pulse as usual. This effectively prevents level 2–level 1 recycling and was found

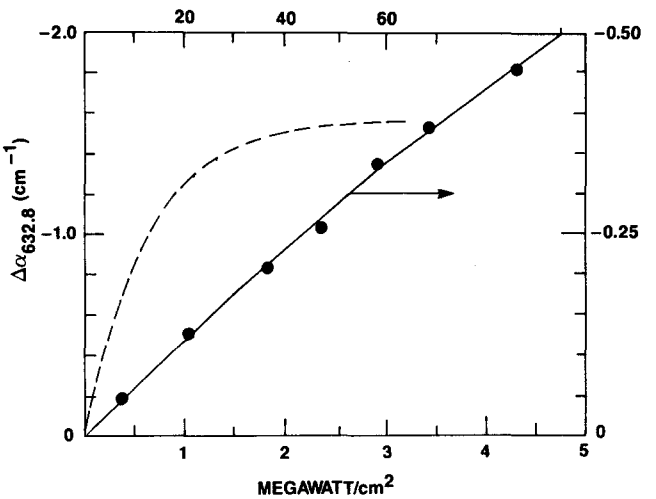

FIG. 5. The calculated (dashed and solid lines) and measured (dots) $\Delta\alpha$ values at 632.8 nm for GSGG:Cr^{3+}. The incident power was calculated from the measured pump energy and the 0.85 μs pulse duration.

to have the effect of increasing σ_1 by 10%. This minor effect is probably a result of restricting data to the low power region and of choosing a probe wavelength for which $\sigma_0 \gg \sigma_1$; consequently, we consider the assumption of level 2→level 1 relaxation not critical to the calculation of n_1.

The full σ_1 and σ_0 spectra for GSGG:Cr^{3+} are compared in Fig. 6. The σ_1 spectrum in the visible was extracted from the $\Delta\alpha$ spectrum using the values for σ_1 and σ_0 at 632.8 nm derived earlier, and the UV and near IR band cross sections were obtained by measuring their ratios relative to the visible band. It should be mentioned that the residual ESA absorption in the region 15 000–17 000 cm^{-1} may not be real. Cumulative systematic errors in the parameters used to evaluate n_1 could make the σ_1/σ_0 ratio in this region appear too high, and reducing n_1/N from 0.090 as demanded by Eq. (6) to 0.075 still produces a sensible visible σ_1 spectrum. On the other hand, increasing n_1/N to 0.11 clearly distorts the σ_1 spectrum. For these reasons, the peak ESA cross sections are estimated to have an accuracy of $\pm$25% and they are 7.9×10^{-18} cm^2 (32 000 cm^{-1}), 3.5×10^{-20} cm^2 (19 200 cm^{-1}), and 4.7×10^{-21} cm^2 (9000 cm^{-1}).

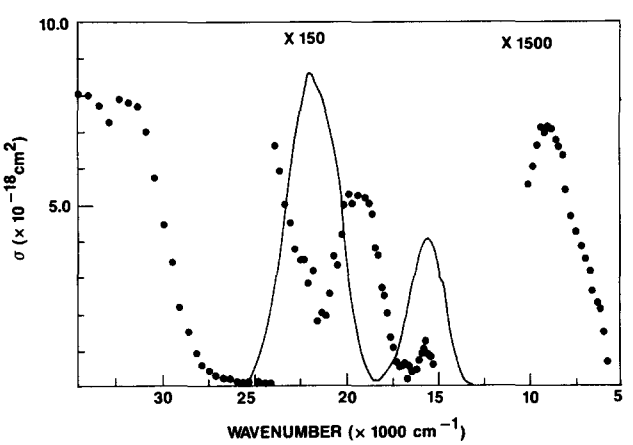

FIG. 6. ESA (dots) and GSA (line) cross sections for GSGG:Cr^{3+}.

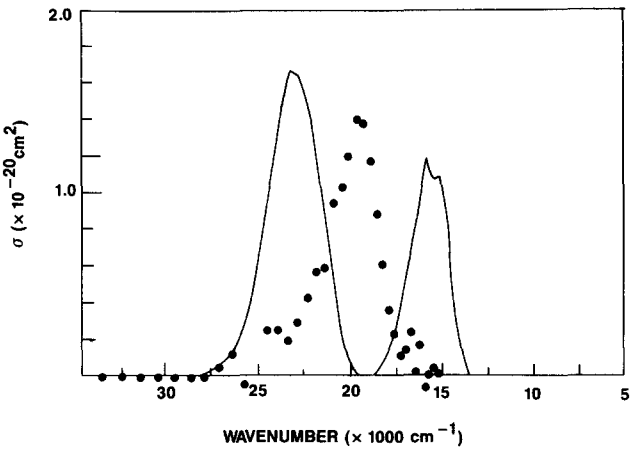

FIG. 7. ESA (dots) and GSA (line) cross sections for $K_2NaScF_6:Cr^{3+}$.

The σ_1 and σ_0 spectra for $K_2NaScF_6:Cr^{3+}$ are shown in Fig. 7. Because of the close similarity between the GSGG:Cr^{3+} and elpasolite:Cr^{3+} visible spectra, σ_1 for the latter spectrum was extracted from the difference spectrum by estimating n_1/N to be 0.027 for the data in Fig. 2 with the peak 1.4×10^{-20} cm^2 at 19 400 cm^{-1}. The noise in the wings of this ESA band reflects the low S/N ratio for the data, it is about a factor of 5 lower than for the GSGG:Cr^{3+} data due to lower cross sections and a smaller probe path length, and it is likely that the near IR band ESA band of elpasolite:Cr^{3+} eluded detection for these reasons.

VI. GSGG:Cr^{3+} LASER TUNING RANGE

The material GSGG:Cr^{3+} operates as a tunable laser on the $^4T_{2g}\rightarrow{}^4A_{2g}$ transition, and it is worthwhile to compare its reported tuning range of 742–842 nm[13] to whatever limits can be inferred from the present ESA results. Inspection of Fig. 6 suggests that the short wavelength tuning limit will be determined by hot absorption associated with GSA in a manner analogous to tunable dye lasers. The long wavelength limit, on the other hand, will be determined by the broad near infrared ESA band. To make a quantitative comparison between stimulated emission and absorption, the stimulated emission cross sections were calculated from the GSGG:Cr^{3+} fluorescence using McCumber's theory.[14] The fluorescence function $f(\bar{\nu})$ for an isotropic emitter when normalized to the radiative lifetime τ_R, as shown in Eq. (10), is related to the stimulated emission cross section by Eq. (11),

$$1/\tau_R = 8\pi \int_{\bar{\nu}} f(\bar{\nu})d\bar{\nu}, \tag{10}$$

$$\sigma(\bar{\nu}) = f(\bar{\nu})/(\bar{\nu}n)^2. \tag{11}$$

Using 120 μs for τ_R and 1.94 for the GSGG refractive index, the stimulated emission spectrum was calculated from the corrected fluorescence as shown in Fig. 8 where the peak emission cross section is 8.4×10^{-21} at 760 nm. Also shown in Fig. 8 is the near infrared ESA band and a fit of this complex band to a double Gaussian as defined by Eq. (12),

$$\sigma(\bar{\nu}) = \sum_{i=1}^{2} \sigma(\bar{\nu}_0)\exp[-(\bar{\nu}-\bar{\nu}_0)^2/2\Delta\bar{\nu}^2]. \tag{12}$$

The fitting parameters are listed in Table I. When the double Gaussian fit is extrapolated into the fluorescence region, the ultimate long wavelength tuning limit of the GSGG:Cr^{3+} laser is estimated to be 11 125 $\pm$ 250 cm^{-1} where the error reflects $\pm$25% uncertainty in peak cross sections of both emission and absorption. The observed tuning limit at 11 857 cm^{-1} (842 nm) is shown as an arrow in Fig. 8. Of course, the latter measurement was not performed in a lossless cavity, so the tuning limit inferred here is at least consistent with the laser results and confers some confidence that the ESA cross sections do not contain large systematic errors.

VII. THE a_{1g} SINGLE COORDINATE MODEL

The most primitive description of an active ion coupled to its lattice is the single configuration coordinate model in which all lattice–ion interactions are approximated by cou-

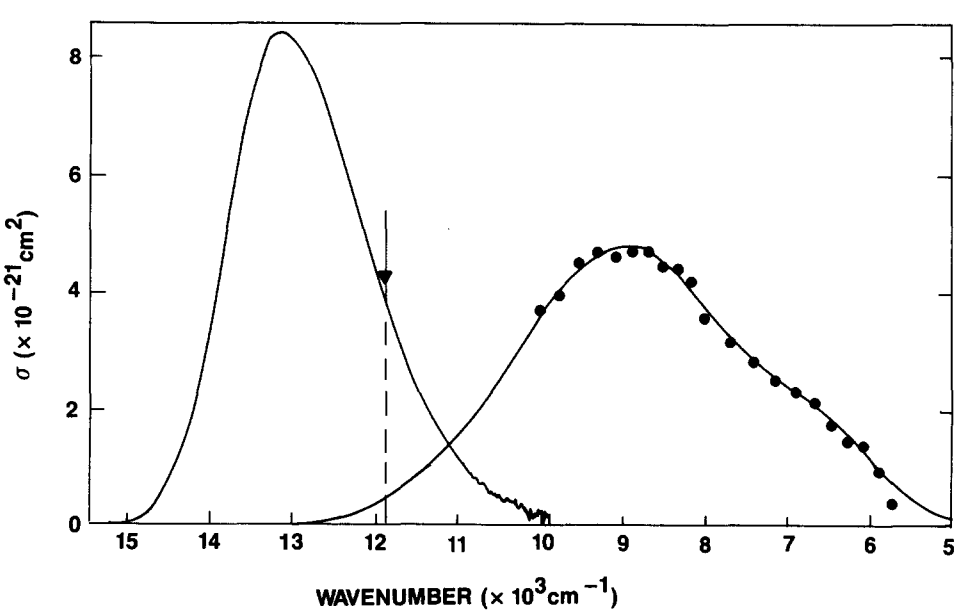

FIG. 8. Stimulated emission cross sections (left) and ESA cross sections (dots) for GSGG:Cr^{3+}. The arrow at 11 875 cm^{-1} is the reported (Ref. 13) tuning limit of the GSGG:Cr^{3+} laser and the fit to the ESA data is a double Gaussian defined in Table I.

TABLE I. Double Gaussian parameters for near IR ESA bands.

	Band 1	Band 2
$\sigma(\bar{\nu}_0)$	4.8×10^{-21} cm^2	1.0×10^{-21} cm^2
$\bar{\nu}_0$	8980 cm^{-1}	6500 cm^{-1}
$\Delta\bar{\nu}$	1350 cm^{-1}	700 cm^{-1}

pling to a single frequency phonon. In spite of its extreme simplicity, the model does have merit in providing a qualitative and occasionally a quantitative description of phonon broadened electron transitions. Here it will be applied to the comparatively well documented case of Cr^{3+} in order to assess its usefulness in describing the ESA spectra of transition metal ions, a task difficult to do rigorously. Our specific aims are to understand the differences between ESA from the ^2E_g and $^4T_{2g}$ states of Cr^{3+} in terms of the number and energies of transitions, and beyond that to predict the ESA transition bandwidths.

Single configuration coordinate diagrams were constructed by taking the total energy of a state to be the sum of an electronic term and an harmonic oscillator term as shown in Eq. (13),

$$E = E_{el}(\Delta r) + 3M\omega^2\Delta r^2. \tag{13}$$

For concreteness, the diagrams were prepared with ligand field parameters derived from the spectrum of the CrF_6 cluster in K_2NaScF_6, and the form of the harmonic potential in Eq. (14) is appropriate for the octahedral a_{1g} vibration[15] where M is the mass of one fluorine, Δr is the displacement of the Cr–F internuclear separation from its equilibrium value r_0, and $\hbar\omega$ is the a_{1g} energy. The electronic term $E_{el}(\Delta r)$ was calculated by diagonalizing the Tanabe–Sugano matrices[16] at discrete values of Δr under the approximation that Dq is proportional to r^{-5} and that B and C are independent of Δr. The hydrostatic pressure results mentioned in Sec. III indicate that this approximation does accurately describe the effects of lattice compression on ligand field parameters. The resulting a_{1g} coordinate diagram for the Cr^{3+} four quartet states [$^4A_{2g}$, $^4T_{2g}$, $^4T_{1g}(a)$, $^4T_{1g}(b)$] and the ^2E_g is shown in Fig. 9. Notice that this treatment produces upper quartet state potential energy surfaces which are offset with respect to the ground state and must lead to fluorescence with an appreciable Stokes shift. Invoking the semiclassical description of radiative transitions[17] permits the construction of spectra from the coordinate diagrams. The vertical energy difference between the initial state potential minimum and the terminal state of a transition gives the first moment m_1 of the band. This energy can be written in terms of the Huang–Rhys parameter S and the energy Ω_0 separating the state minima as shown in Eq. (14),

$$m_1 = S\hbar\omega + \Omega_0, \tag{14}$$

$$m_2^2 = S(\hbar\omega)^2 \coth(\hbar\omega/2kT). \tag{15}$$

The second moment m_2 at temperature T can be obtained from Eq. (15). These moments determine a Gaussian representation of the line shape function $G(\bar{\nu})$ defined in Eq. (16), and plotted

$$G(\bar{\nu}) = \frac{1}{\sqrt{2\pi}m_2}\exp[-(\bar{\nu}-m_1)^2/2m_2^2] \tag{16}$$

vertically on the right of Fig. 9 for the two spin allowed ESA transitions from $^4T_{2g}$ to $^4T_{1g}(a)$ and $^4T_{1g}(b)$.

The choice of $\hbar\omega$ used to construct Fig. 9 requires elaboration. The a_{1g} energy for the CrF_6 cluster in elpasolite is close to 568 cm^{-1},[18] and when this value was used for the harmonic oscillator energy in Eq. (13) the fluorescence line

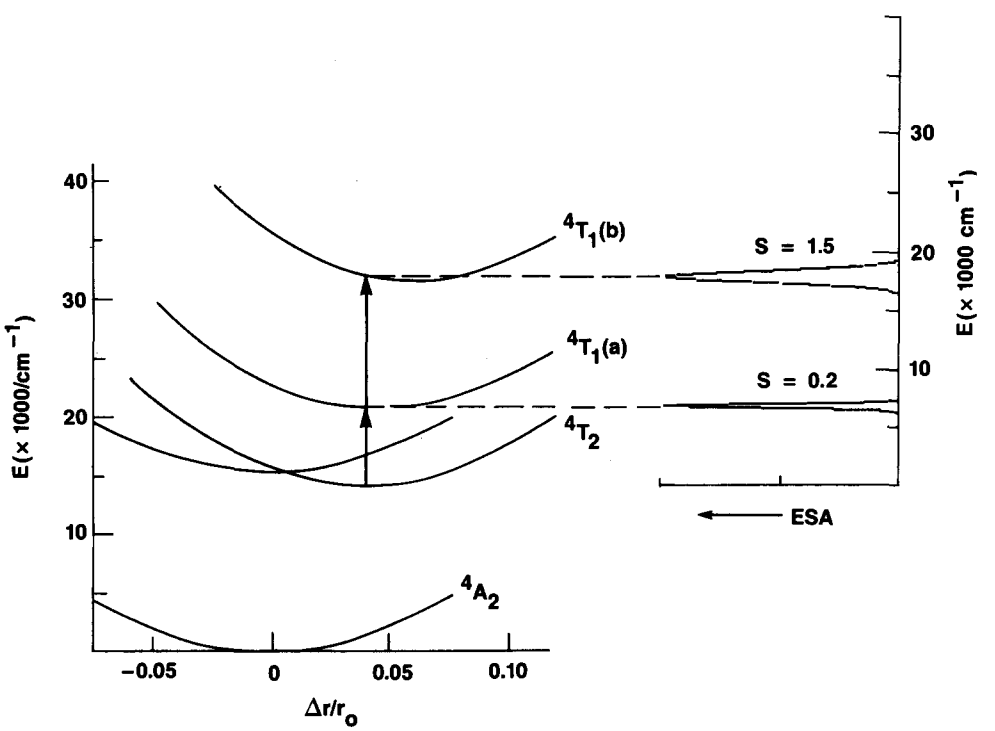

FIG. 9. Single configuration coordinated diagram appropriate for the quartet states of a d^3 ion with $Dq = 1560$ cm^{-1}, $B = 794$ cm^{-1}, $C = 3230$ cm^{-1}, $T = 300$ K, and $\hbar\omega = 330$ cm^{-1}. The value for $r_0 = 0.207$ nm was estimated from the unit cell constant and ionic radii. The calculated ESA spectrum is on the right.

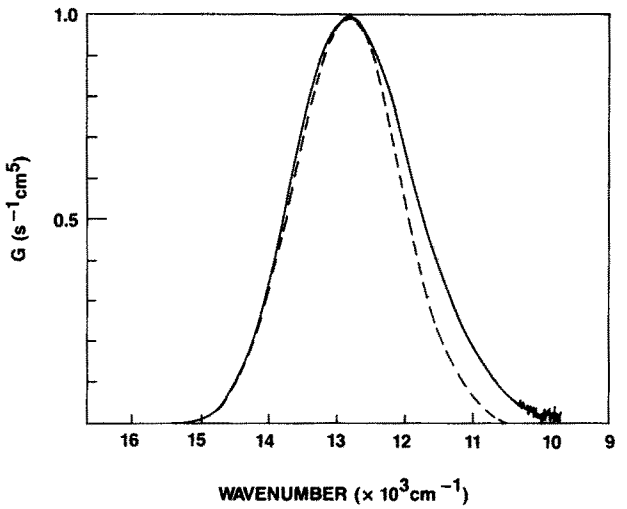

FIG. 10. Comparison of the measured (solid line) line shape function $G(\nu)$ for $K_2NaScF_6:Cr^{3+}$ fluorescence and the $G(\nu)$ (dashed line) calculated from Fig. 9.

shape given by Eq. (16) was a poor match to the observed lineshape $G(\bar{\nu}) = I(\bar{\nu})/\bar{\nu}^4$ where $I(\bar{\nu})$ is the fluorescence spectrum. Accordingly, $\hbar\omega$ was varied to reproduce the observed line shape and the optimum fit was found for $\hbar\omega = 330\,\mathrm{cm}^{-1}$ as shown in Fig. 10. This new coordinate no longer has any relationship with the a_{1g} mode but now represents some average vibration only useful for calibrating the configuration coordinate diagram to real spectra. Table II lists the calculated and observed m_1 and $2m_2^{1/2}$ values for electronic transitions between quartet states in elpasolite:Cr^{3+} and includes the two lowest energy GSGG:Cr^{3+} ESA bands. The energies of the two ligand field ESA bands are calculated to be 75%–90% of the observed values and the bandwidths of the fluorescence and the three GSA bands are within 70%–90% of observed values. To this extent, the configuration coordinate diagram constructed with $\hbar\omega = 330\,\mathrm{cm}^{-1}$ roughly replicates the spectra. However, the calculated ESA bandwidths are spectacularly in error, the $^4T_{1g}(a) \leftarrow {}^4T_{2g}$ and the $^4T_{1g}(b) \leftarrow {}^4T_{2g}$ transitions are calculated to have only 10% and 35%, respectively, of the observed bandwidths. Since the breadth of phonon broadened ESA transitions critically influence predictions regarding laser performance, this result must be regarded as a serious limitation of the model and highlights the need for a more rigorous approach to calculating bandwidths of transitions between degenerate ligand field states.

TABLE II. First and second moments of Cr^{3+} optical transitions (cm^{-1}).

	Observed		Calculated	
Transition	m_1	$2m_2^{1/2a}$	m_1	$2m_2^{1/2a}$
Elpasolite:Cr^{3+}				
$^4T_{2g} \rightarrow {}^4A_{2g}$	12 850	1810	12 850	1580
$^4T_{2g} \leftarrow {}^4A_{2g}$	15 600	2200	...	1750
$^4T_{1g}(a) \leftarrow {}^4A_{2g}$	22 990	2900	...	2070
$^4T_{1g}(b) \leftarrow {}^4A_{2g}$	35 090	3320	35 730	2900
$^4T_{1g}(a) \leftarrow {}^4T_{2g}$	...	...	6 830	350
$^4T_{1g}(b) \leftarrow {}^4T_{2g}$	19 400	2700	17 940	980
GSGG:Cr^{3+}				
$^4T_{1g}(a) \leftarrow {}^4T_{2g}$	9 000	3200	...	...
$^4T_{1g}(b) \leftarrow {}^4T_{2g}$	19 200	2600	...	...

[a] This is the full bandwidth at $I = I_0 \exp(-0.5)$.

In spite of its limitations, it is nevertheless useful to construct the coordinate diagram appropriate for ESA transitions from the ^2E_g state to higher energy doublets. This is done in Fig. 11 which shows only the nine transitions (out of a possible 15) that are expected to have near infrared or visible absorption bands. It is clear from a comparison of Figs. 9 and 11 that a major qualitative difference exists between ESA within the doublet and quartet manifolds. To the extent that spin is a valid selection rule, ESA from the $^4T_{2g}$ state of a low field Cr^{3+} ion consists of only two bands attributable to ligand field transitions and the ESA spectra of elpasolite:Cr^{3+} and GSGG:Cr^{3+} shown in Sec. V demonstrate that this picture is correct. On the other hand, ESA from the ^2E_g state of a high field Cr^{3+} ion consists of a far more congested spectrum with transitions blanketing the visible. This picture has also been shown to be correct by Fairbank *et al.*[2] who measured the ESA of emerald:Cr^{3+} at 113 K. The ^2E–$^4T_2$ gap in emerald is 350 cm^{-1} so at this temperature the ^2E has 97% population at thermal equilibrium. The emerald:Cr^{3+} spectra (π and σ) above 15 000 cm^{-1} are compared with elpasolite:Cr^{3+} in Fig. 12, and we attribute the major differences seen in Fig. 12 between the ESA of Cr^{3+} in these hosts to a change in the identity of the lowest excited state from $^4T_{2g}$ in elpasolite to ^2E in emerald. Because of the close spacing between doublet–doublet transitions, these bands are poorly resolved and no attempt will be made here to assign the bands; instead Fairbank *et al.*[2] should be consulted for their interpretation of the emerald:Cr^{3+} data.

VIII. CONCLUSION

The principal result reported here is that a major qualitative difference exists between the ESA spectra of Cr^{3+} ions having $^4T_{2g}$ and ^2E_g lowest excited states, and this difference can be interpreted in terms of the electron spin selection rule. In the case of low field Cr^{3+}, only two spin allowed transitions are possibles from $^4T_{2g}$ to higher lying ligand field states, one to the $^4T_{1g}(a)$ in the near infrared and a second to the $^4T_{1g}(b)$ in the visible. Consistent with this expectation, broad infrared ESA bands centered near 9000 cm^{-1} were located in both GSGG:Cr^{3+} and GSAG:Cr^{3+}, and visible bands near 19 000 cm^{-1} were located in the elpasolite as well as the garnets. The ESA spectrum of the elpasolite shows further that no additional ligand field transitions are present up to at least 40 000 cm^{-1}. In addition, the spectral region between the $^4T_{1g}(a)$, $^4T_{1g}(b) \leftarrow {}^4T_{2g}$ transitions, roughly the 11 000–16 000 cm^{-1} fluorescence region, is expected to be relatively free of absorption. This could not be confirmed in the present study, but recently Huber *et al.*[7] have compared the gain cross section of the GSGG:Cr^{3+} laser with the stimulated emission cross section calculated using McCumber's theory and found them to be substantially

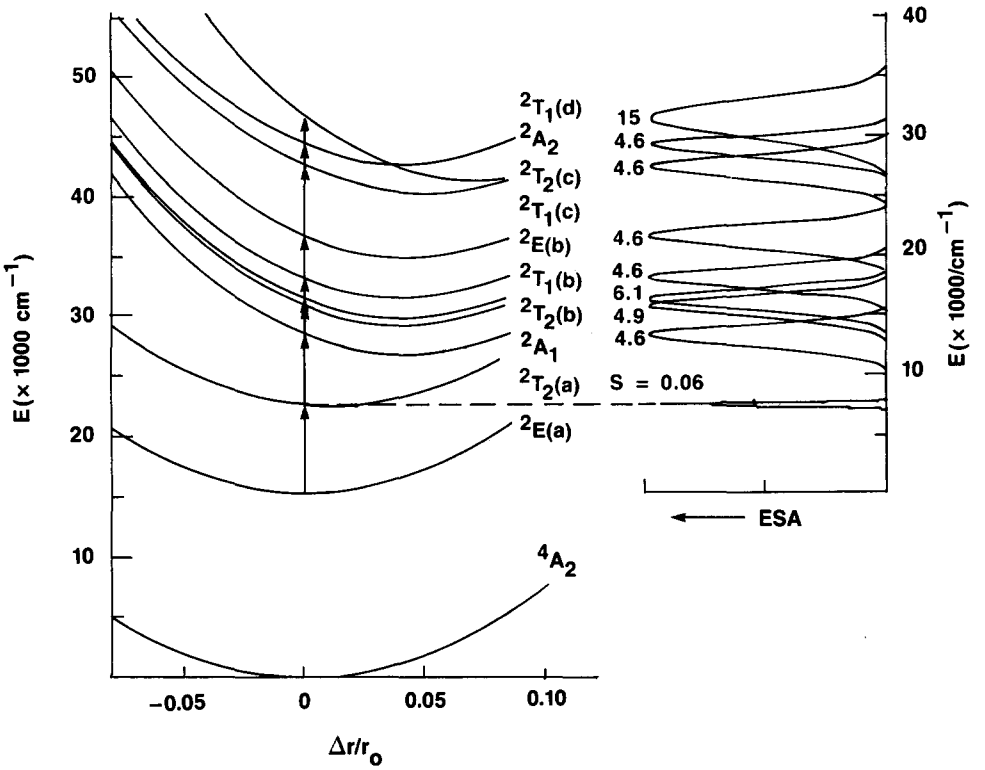

FIG. 11. Single configuration coordinate diagram and calculated ESA spectrum for doublet states of a d^3 ion. The ligand field parameters are the same as in Fig. 9.

identical at their maxima which implies an absence of ESA in the vicinity of the fluorescence.

In the case of high field Cr^{3+}, nine transitions between ligand field states are expected to produce a congested ESA spectrum in visible and near infrared, and the spectrum of emerald[2] confirms that this is true for energies greater than 14 000 cm^{-1}. In the region of thermally induced $^4T_2 \rightarrow {}^4A_2$ fluorescence, the $^2A_1 \leftarrow {}^2E(a)$ ESA transition could be detrimental to laser gain, but unfortunately, this transition was not clearly identified in the emerald work. However, in the closely related case of alexandrite in which the $^4T_2$ lies 850 cm^{-1} above the ^2E, Shand *et al.*[3] find an ESA minimum at the stimulated emission peak near 13 000 cm^{-1}. Evidently, the $^2A_1 \leftarrow {}^2E(a)$ and $^2T_1(b), {}^2T_2(b) \leftarrow {}^2A_1$ transitions are sufficiently well separated to permit a useful gain cross section to exist in the fluorescence region. This result could not have been predicted with any single coordinate mode such as outlined in Sec. VII.

Despite the limitations of the single coordinate model in dealing with the bandwidths of ESA transitions, grafting a simple harmonic potential onto ligand field state energies does provide a useful framework for assigning ESA spectra by correctly predicting the number and approximate energies of ESA bands. Since it is only correct to expect coupling to a single a_{1g} coordinate to be an appropriate description for transitions between singlet states, it should not be too surprising that bandwidths cannot be reproduced by the model. In particular, the $T_1 \leftarrow T_2$ infrared transition is between orbital triplets, a Jahn–Teller case which has not yet been treated theoretically and which certainly should exhibit strong coupling to modes of higher degeneracy than a_{1g}.

Finally, we consider the origin of the intense near ultraviolet ESA bands observed in GSGG:Cr^{3+} and GSAG:Cr^{3+}. The peak cross sections of these bands are nearly 10^{-17} cm^2 indicating an electric dipole allowed transition which cannot have a ligand field state as the terminal

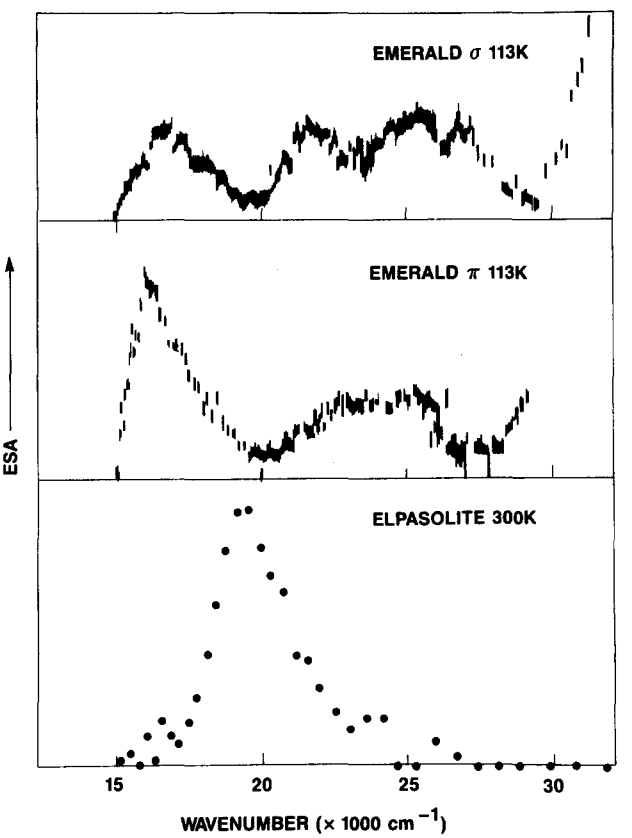

FIG. 12. Comparison of the visible and UV ESA spectra of elpasolite:Cr^{3+} (low field) and emerald (Ref. 2) (high field).

level. Strong transitions of this type have been commonly observed in the optical spectra of transition metals and are usually assigned to interconfigurational (e.g., $3d \rightarrow 4s$) or charge transfer type transitions,[19] both of which can be parity allowed in centrosymmetric point group symmetries. For Cr^{3+}, an interconfiguration transition is unlikely in this energy region, even from the ${}^4T_{2g}$ excited state, because the binding energy difference between $3d$ and $4s$ atomic orbitals is about 10^5 cm^{-1} which even if corrected for ligand field effects leads to a much higher energy transition than observed. Therefore, a charge transfer transition with its characteristic sensitivity to the identity of the transition metal ligand is much more likely. The ionization potential of the ligand is usually cited as a critical parameter in determining the energy of charge transfer band, and, accordingly, one expects oxides to have lower energy charge transfer transitions than fluorides. This is true for the case of Cr^{3+} in which the energy of the unobserved fluoride charge transfer transition is a minimum of 18 000 cm^{-1} higher than in GSGG. Even in the two garnets, the position of this band is sensitive to the identity of the next nearest neighbors and blue shifts 800 cm^{-1} when Al replaces Ga. This shift is in accord with the higher ionization potential of Al^{3+} with respect to Ga^{3+}. The appearance of Cr^{3+} ESA charge transfer bands is not limited to oxide garnets as the onset of these transitions are clearly visible in the ESA spectra of emerald at 27 000 cm^{-1} and MgO at 29 000 cm^{-1}.[2] These bands occur at 5000 and 7000 cm^{-1} higher energy than in GSGG and reflect the higher ionization potential expected of O^{2-} in these lattices.

Since the charge transfer state can be viewed as the oxidation of a ligand creating a hole and the reduction of Cr^{3+} to Cr^{2+}, it is of interest to know if this state lies within the conduction band of the host. If it does, the charges may have appreciable mobility and decay by being trapped at defect centers, rather than hole-Cr^{2+} recombination, and lead to color center formation such as has been reported for flash lamp pumped GSGG:Cr^{3+} lasers.[20] A charge transfer state within the conduction band should also give rise to appreciable two photon photoconductivity analogous to the one photon photoconductivity reported for charge transfer excitation in rare earths.[21]

ACKNOWLEDGMENT

The authors wish to thank Professor R. H. Bartram of the University of Connecticut for helpful discussions regarding the application of the single configuration coordinate model to ligand field states.

[1] P. T. Kenyon, L. J. Andrews, B. C. McCollum, and A. Lempicki, IEEE J. Quant. Electron. **QE-18**, 1189 (1982).
[2] W. M. Fairbank, Jr., G. K. Klauminzer, and A. L. Schawlow, Phys. Rev. B **11**, 60 (1975), and references therein to early work on ruby.
[3] M. L. Shand and J. C. Walling, IEEE J. Quant. Electron. **QE-18**, 1152 (1982).
[4] M. L. Shand and H. P. Jenssen, IEEE J. Quant. Electron. **QE-19**, 480 (1983).
[5] R. A. Krause, I. Traubjerg, and C. J. Ballhausen, Chem. Phys. Lett. **3**, 297 (1969).
[6] A. M. Bonch-Bruevich, T. K. Razumova, and Ya. A. Imas, Opt. Spectrosc. **20**, 575 (1966).
[7] B. Struve, G. Huber, V. V. Laptev, I. A. Shcherbakov, and E. V. Zharikov, Appl. Phys. B **30**, 117 (1983); B. Struve and G. Huber, J. Appl. Phys. **57**, 45 (1985).
[8] D. Mateika, in *Current Topics in Materials Science, Vol. II*, edited by E. Kaldis (North-Holland, Amsterdam, 1984), p. 228.
[9] L. J. Andrews (unpublished results).
[10] J. F. Dolan and R. H. Bartram, Dept. of Physics, Univ. of Connecticut (private communication).
[11] B. Struve and G. Huber, Appl. Phys. B **36**, 195 (1985).
[12] R. H. Bartram, J. C. Charpie, L. J. Andrews, and A. Lempicki, Phys. Rev. B (to be published).
[13] G. Huber, Technical Digest, OSA Topical Meeting on Tunable Solid State Lasers, Arlington, VA, May 16–17, 1985, THA3.
[14] D. E. McCumber, Phys. Rev. **134**, A299 (1964); **136**, A954 (1964).
[15] C. W. F. T. Pistorius, J. Chem. Phys. **29**, 1328 (1958); K. Nakamoto, *Infrared Spectra of Inorganic and Coordination Compounds* (Wiley, New York, 1963), pp. 10–14, 45–56.
[16] D. S. McClure, in *Solid State Physics, Vol. 9*, edited by F. Seitz and D. Turnbull (Academic, New York, 1959), p. 399.
[17] D. Curie, in *Optical Properties of Ions in Solids*, edited by B. DiBartolo, Nato Advanced Study Institute, Erice, Italy, 1974 (Plenum, New York, 1975), p. 71.
[18] P. Greenough and A. G. Paulusz, J. Chem. Phys. **70**, 1967 (1979).
[19] D. S. McClure, in *Electronic States of Inorganic Compounds: New Experimental Techniques*, edited by P. Day, Nato Advanced Study Institute, Oxford, 1974 (Reidel, Dordrecht, Holland, 1975), p. 113.
[20] M. J. P. Payne and E. W. Evans, Technical Digest, OSA Topical Meeting on Tunable Solid State Lasers, Arlington, VA, May, 1985, FA4; R. C. Simpson and K. L. Schepler, FA5.
[21] C. Pedrini, F. Gaume-Mahn, and D. S. McClure, in *The Rare Earths in Modern Science and Technology, Vol. 3*, edited by G. J. McCarthy, H. B. Silber, and J. J. Rhyne (Plenum, New York, 1982), p. 165.